Chapter 8

Back to Basics: Nonlinear Dynamics and Complete Stability

8.1. A Glimpse of Things to Come

All CNN templates we have investigated so far share the common property that regardless of the inputs, initial states, and boundary conditions, all transient dynamics eventually converge to some *dc* equilibrium state after some *settling time* $k\tau_{CNN}$, where τ_{CNN} is the time constant of a single cell, and $k \approx 5 \sim 10$. Such CNN's are said to be completely stable and represent the workhorse of most current CNN applications. Indeed, almost all current CNN analogic programs are developed under the assumption that all CNN templates (instructions) called for in the program are completely stable. However, we will see in the following sections that *not all* CNN's are completely stable. Indeed, some CNN templates will give rise to an *oscillatory periodic* steady state behavior. Others can even exhibit an eternally transient (not periodic) phenomenon called *chaos*.

While the majority of current CNN applications require *constant* dc (gray-scale) outputs, future applications will no doubt exploit the immense potentials of the relatively unexplored terrains of oscillatory and chaotic operating regions. A glimpse of some such novel CNN applications in these regions will be given in Chapter 18. In this chapter, we will derive several general mathematical criteria for complete stability. To appreciate the need for such criteria, we will present first a simple example of an *oscillatory* CNN in section 8.2, and a *chaotic* CNN in section 8.3.

8.2. An Oscillatory CNN with Only two Cells

Consider a 2-cell CNN characterized by zero boundary conditions and the following templates:

$$A = \begin{array}{|c|c|c|}\hline 0 & 0 & 0 \\ \hline \beta & \alpha & -\beta \\ \hline 0 & 0 & 0 \\ \hline \end{array} \qquad B = \begin{array}{|c|c|c|}\hline 0 & 0 & 0 \\ \hline 0 & 0 & 0 \\ \hline 0 & 0 & 0 \\ \hline \end{array} \qquad z = \boxed{0}$$

using our earlier notations from section 2.2.6, this MxN=1x2 CNN with feedback synaptic weights $a_{0,-1}=\beta$, $a_{0,0}=\alpha$, and $a_{0,1}=\beta$ can be represented by the signal flow graph shown in Fig.1.

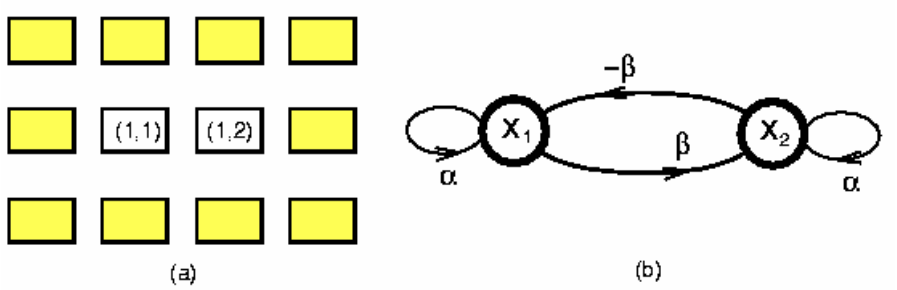

Fig.1 (a) A 1x2 CNN whose virtual boundary cells (shown shaded) are clamped to a zero potential: $y_{0,0}= y_{0,1}= y_{0,2}= y_{0,3} = y_{1,0}= y_{1,3}= y_{2,0}= y_{2,1}= y_{2,2}= y_{2,3}=0$*. (b) Corresponding signal flow graph*

The state equations for this CNN is given by:

$$\begin{aligned} \dot{x}_1 &= - x_1 + \alpha y_1 - \beta y_2 \\ \dot{x}_2 &= - x_2 + \alpha y_2 + \beta y_1 \end{aligned} \tag{8.1}$$

where we neglect the row index for simplicity. Here, the output y_i is related to the state x_i by the standard nonlinearity

$$y_i = f(x_i) = 0.5| x_i +1| - 0.5| x_i -1| \tag{8.2}$$

which is shown graphically in Fig.2 for convenience.

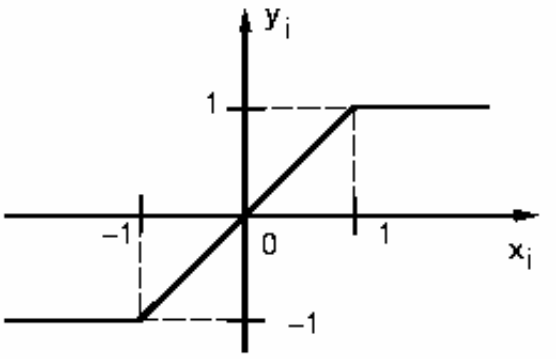

Fig.2 The standard CNN piecewise-linear output characteristic.

The solution waveforms of Eq.(8.1) corresponding to $\alpha = 2$, $\beta = 2$, and initial condition $x_1(0) = 0.1$ and $x_2(0) = 0.1$ are shown in Figs.3(a) and 3(b). Observe that instead of converging to a dc equilibrium point as in all of our previous examples, the state variables x_1 and x_2 converge to a *periodic* waveform, which is more clearly seen by plotting the associated *trajectory* in the x_1-x_2 plane, as shown in Fig.3(c). Each point along the trajectory, which starts from $(x_1, x_2) = (0.1, 0.1)$ at t=0 in Fig.3(c) is parameterized by time but is not shown in the figure because, here, we are interested only in the relationship between $x_1(t)$ and $x_2(t)$ as $t\rightarrow\infty$, namely, a *closed contour* called a *limit*

cycle. Since the trajectory from (0.1, 0.1) does not converge to an equilibrium (x_{1Q}, x_{2Q}), this CNN is *not* completely stable.

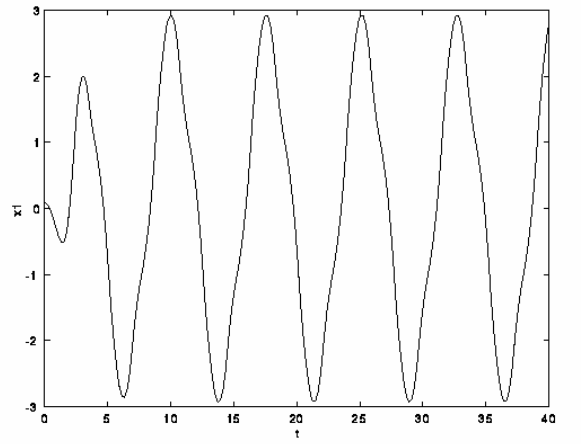

(a)

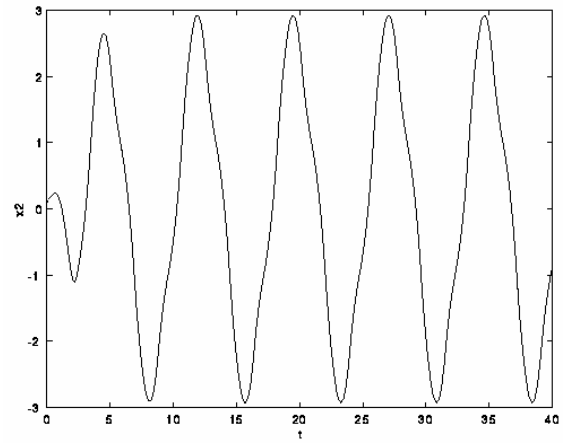

(b)

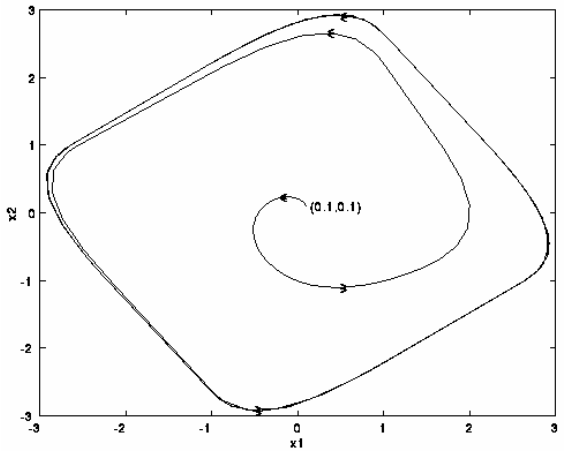

(c)

Fig.3 Periodic solution waveforms of $x_1(t)$ and $x_2(t)$ and the corresponding trajectory for $\alpha=2$, $\beta=2$, $x_1(0)=0.1$ and $x_2(0)=0.1$.

For this simple example, we can prove that all trajectories starting from any initial state except the origin will converge to a limit cycle. We will present the details of this proof in order to introduce the uninitiated readers to some elementary aspects of *nonlinear qualitative analysis*. The first step in analyzing the dynamics of an *autonomous* CNN (i.e., where the time variable t does not appear on the right-hand side of the state equation) is to find the location of all equilibrium points Q_i, i=1,2,...,q, such that $\dot{x}_1(Q_i) = 0$ and $\dot{x}_2(Q_i) = 0$, where $\dot{x}_j(Q_i)$ denotes $\dot{x}_j(t)$ evaluated at $x_i = x_{Q_i}$ Hence, upon setting Eq.(8.1) to 0, the equilibrium points of this 2-cell CNN are the solutions of:

$$- x_1 + 2f(x_1) - 2f(x_2) = 0 \qquad (8.3a)$$

$$- x_2 + 2f(x_2) + 2f(x_1) = 0 \qquad (8.3b)$$

Since the piecewise-linear function $f(x_i)$ in Fig.3 has 3 segments, the x_1-x_2 state space can be partitioned into 9 rectangular regions R(i,j), i,j=1,2,3, as shown in Fig.4, where the state equation (1) reduces to a linear equation in each region. In particular, the equilibrium equation (3) reduces to 2 linear algebraic equations in each region R(i,j) and the equilibrium point Q(i,j) can be trivially calculated. If Q(i,j) falls within region R(i,j), then it is a valid equilibrium point. If Q(i,j) falls outside of R(i,j), it is a "virtual" equilibrium point and is simply discarded. The above "brute-force" procedure can be easily programmed to find all equilibrium points of any MxN CNN. However, the computation time would grow exponentially with MN so that it becomes impractical when MN is large.

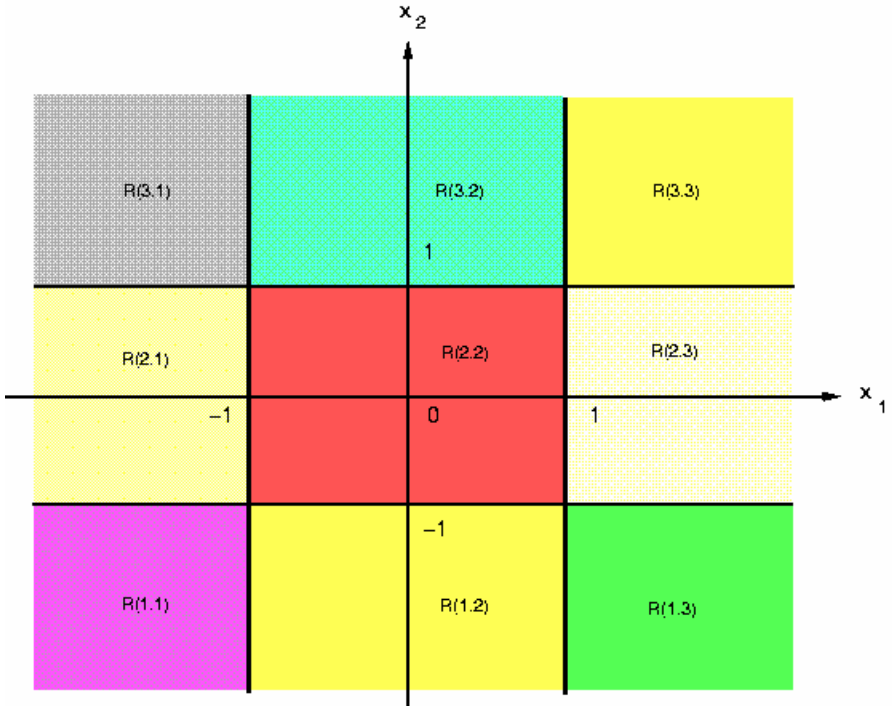

Fig.4. The dynamics of the 2-cell CNN in Fig.1 is linear in each region R(i,j).

In view of the simplicity of Eq.(8.3), the *following algebraic analysis* can be made to determine first those regions in Fig.4 which have valid equilibrium points:

Step 1. Central strip $|x_1|<1$ (regions R(1,2), R(2,2), and R(3,2) in Fig.4):

In the strip $| x_1 |<1$, we can write $f(x_1) = x_1$ so that Eq.(8.3a) becomes $- x_1 + 2x_1 - 2f(x_2) = 0$. Consequently, $|f(x_2)| = |x_1|/2 < 0.5$ and hence $f(x_2) = x_2$. Equation (8.3) reduces in this case to:

$$\begin{aligned} &- x_1 + 2x_1 - 2x_2 =0 \\ &- x_2 + 2x_2 + 2 x_1 =0 \end{aligned} \qquad (8.4)$$

Since $(x_1, x_2) = (0,0)$ is the *unique* solution of Eq.(8.4), only region R(2,2) in the central strip has an equilibrium point; namely, the origin.

Step 2. Left strip $x_1< -1$ (regions R(1,1), R(2,1), and R(3,1) in Fig.4):

In the strip $x_1< -1$, we can write $f(x_1) = -1$ so that Eq.(8.3b) becomes $- x_2 + 2f(x_2) - 2 = 0$. Solving this equation for x_2, we find $x_2= -4$ for region R(1,1) the only solution of Eq.(8.3b) (the other two solutions $x_2=2$ for region R(2,1) and $x_2=0$ for region R(3,1) are both *virtual* solutions). But $x_2= -4$ implies $f(x_2)=-1$ so that Eq.(8.3a) in the left strip gives $-x_1-2+2=0$, or $x_1=0$, which is outside of the left strip. Hence $x_2=-4$ is a virtual solution for Eq.(8.3). It follows that *there are no equilibrium points in the left strip* $x_1<-1$.

Step 3. Right strip $x_1>1$ (regions R(1,3), R(2,3), and R(3,3) in Fig.4):

In the strip $x_1>1$, we can write $f(x_1) = 1$ so that Eq.(8.3b) becomes $- x_2 + 2f(x_2) +2 = 0$. Solving this equation for x_2, we find $x_2= 4$ for region R(3,3) is the only solution of Eq.(8.3b) (the other two solutions $x_2=-2$ for region R(2,3) and $x_2=0$ for region R(1,3) are both *virtual* solutions). But $x_2= 4$ implies $f(x_2)=1$ so that Eq.(8.3a) in the *right strip* gives $-x_1+2-2=0$, or $x_1=0$, which is outside of the right strip. Hence $x_2=4$ is a virtual solution for Eq.(8.3). It follows that *there are no equilibrium points in the right strip* $x_1>1$.

Steps 1-3 show that Eq.(1) has only one equilibrium point; namely, the origin. To determine the dynamical behavior near the origin, we examine the associated linear equation

$$\begin{aligned} \dot{x}_1 &= x_1 - 2x_2 \\ \dot{x}_2 &= 2x_1 + x_2 \end{aligned} \qquad (8.5)$$

obtained by setting $f(x_1) =x_1$ and $f(x_2)=x_2$ in Eq.(8.1). Since the eigenvalues of the above matrix are given by $\lambda_1=1+j2$ and $\lambda_2=1-j2$, the solution of Eq.(8.5) has the form:

$$\begin{aligned} x_1(t) &= ke^t \cos(2t+\theta) \\ x_2(t) &= ke^t \sin(2t+\theta) \end{aligned} \qquad (8.6)$$

where the constants k and θ depend on the initial condition $x_1(0)$ and $x_2(0)$. Since the trajectory associated with Eq.(8.6) is an "expanding" spiral, as shown in Fig.3(b), and since all solutions of Eq.(8.1) are *bounded* (in view of Theorem 2 of *Chapter 2*), this expanding spiral must necessarily converge to some limiting *closed contour*, for otherwise, the trajectory would intersect itself since there is no room for maneuvering on the x_1-x_2 plane. But no trajectory of an autonomous system of differential equations can intersect itself in view of the *uniqueness* property (Theorem 1 of Chapter 2) -- otherwise we can choose the self-intersection point as our initial condition and obtain 2 different trajectories originating from this point. The above reasoning can be given a formal rigorous proof and the result is called *Poincare-Bendixon* theorem, which is a classic result from the theory of differential equations.[1]

8.3. A chaotic CNN with only 2 cells and one sinusoidal input

Suppose we apply a sinusoidal input $u_{11}(t) = 4.04 \sin(\frac{\pi}{2} t)$ to cell C(1,1) of the 2-cell CNN shown in Fig.1 and choose α=2 and β=1.2 as its parameters. In this case, under the same "zero" boundary conditions as before, the state equation (1) generalizes to the following non-autonomous system of two nonlinear differential equations:

$$\boxed{\begin{aligned} \dot{x}_1 &= -x_1 + 2\,y_1 - 1.2\,y_2 + 4.04 \sin(\tfrac{\pi}{2} t) \\ \dot{x}_2 &= -x_2 + 1.2\,y_1 + 2\,y_2 \end{aligned}} \qquad (8.7)$$

where $y_i = f(x_i)$ is defined by Eq.(8.2). Equation (8.7) is the state equation of a 1x2 CNN with templates

$$A = \begin{array}{|c|c|c|}\hline 0 & 0 & 0 \\ \hline 1.2 & 2 & -1.2 \\ \hline 0 & 0 & 0 \\ \hline \end{array} \qquad B = \begin{array}{|c|c|c|}\hline 0 & 0 & 0 \\ \hline 0 & 1 & 0 \\ \hline 0 & 0 & 0 \\ \hline \end{array} \qquad z = \boxed{0}$$

zero boundary conditions, a sinusoidal input $u_{11}(t)$ to cell C(1,1) and a zero input $u_{12} = 0$ to cell C(1,2). The solution waveforms $x_1(t)$ and $x_2(t)$ corresponding to the initial condition $x_1(0) = 0.1$ and $x_2(0) = 0.1$ are shown in Figs.5(a) and 5(b), respectively. Observe that unlike the periodic waveforms shown earlier in Figs.3(a) and 3(b), these two waveforms do *not* converge to a periodic waveform as $t \to \infty$. The non-periodic nature of $x_1(t)$ and $x_2(t)$ is more clearly seen by examining the associated trajectory shown in Fig.5(c). Observe that the trajectory looks like a never-ending tangle of yarn. To emphasize the non-periodic nature of $x_1(t)$ and $x_2(t)$, Figs.6(a) and 6(b) show the numerically calculated power spectra $X_1(\omega)$ of $x_1(t)$ and $X_2(\omega)$ of $x_2(t)$ have a *broadband, continuous, noise-like character*, which is quite different from that of a periodic signal, which consists of discrete lines corresponding to the harmonic components of its Fourier series expansion. From the theory of the nonlinear dynamics, the noise-like waveforms in Figs.5(a) and 5(b) are said to be *chaotic*, and the associated trajectory is called a *strange*

[1] For a rigorous statement and proof of the Poincare-Bendixon theorem, see P. Hartman, Ordinary Differential Equations, p.151.

attractor because other solutions corresponding to nearby initial conditions will all be "attracted" and converge to the same trajectory.

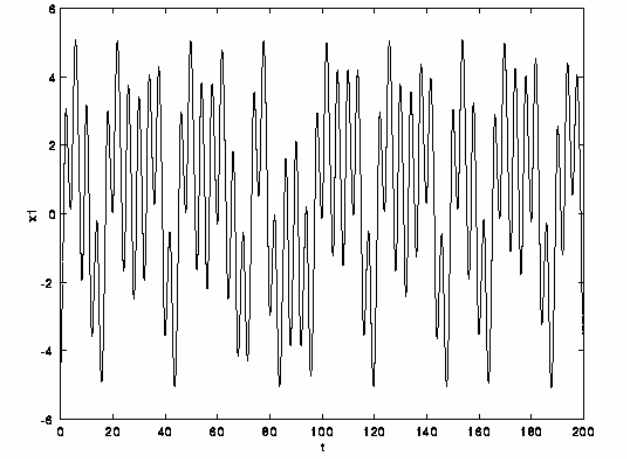

(a)

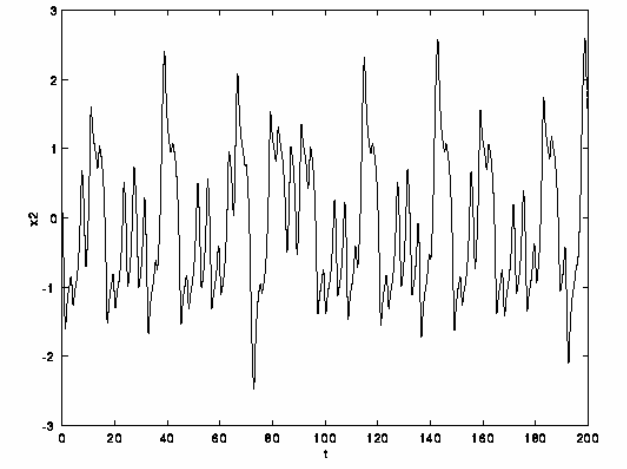

(b)

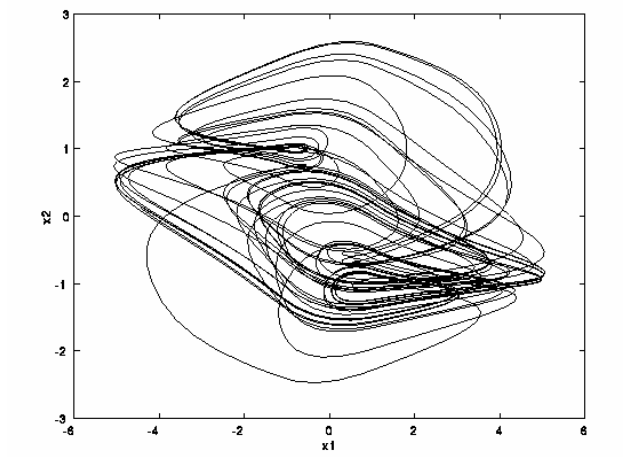

(c)

Fig.5 Chaotic solution waveforms of $x_1(t)$ and $x_2(t)$ and the corresponding trajectory for $\alpha=2$, $\beta = -1.2$, $x_1(0)=0.1$ and $x_2(0)=0.1$.

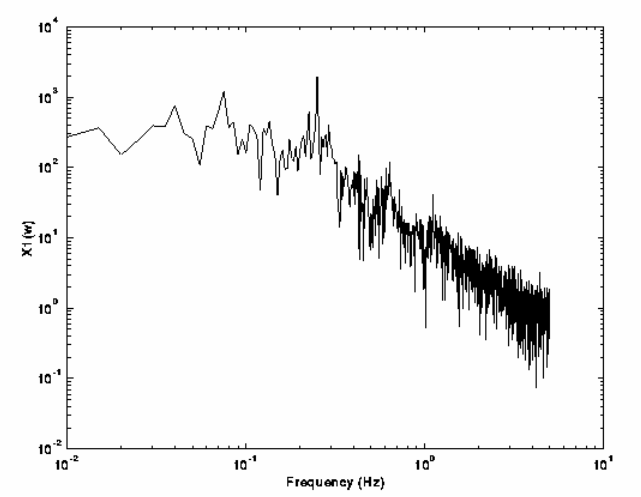

(a)

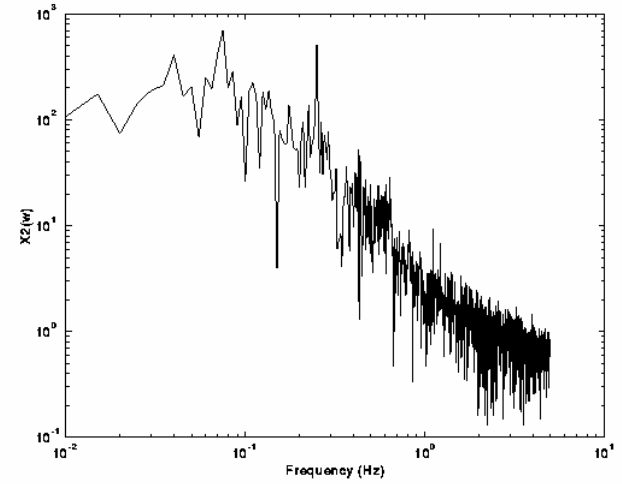

(b)

Fig.6 Frequency power spectra calculated numerically from the chaotic waveforms $x_1(t)$ and $x_2(t)$ in Fig.5.

Even though the strange attractor in Fig.5(c) looks extremely messy, it does possess some orderly geometrical structure, which, in the case of a periodic input, is best seen by sampling only the points on the trajectory once every period of the input waveform. The resulting set of points is called a Poincare cross section, or by an abuse of language, simply *Poincare map* because it was first introduced by the famous French physicist and mathematician Poincare. In this example, the period of the sinusoidal input is T=4. Consequently, if we plot ($x_1(t)$, $x_2(t)$) on the x_1-x_2 plane only at t=0, 4, 8, 12, 16, ... , etc., we would obtain the "sampled" strange attractor in Fig. 7, which is often referred by as a Lady's shoe attractor.[2]

[2]F. Zou and J.A. Nossek, "A chaotic attractor with cellular neural network," *IEEE Trans. on Circuits and Systems*, vol.38, no.7, pp.811-812, 1991.

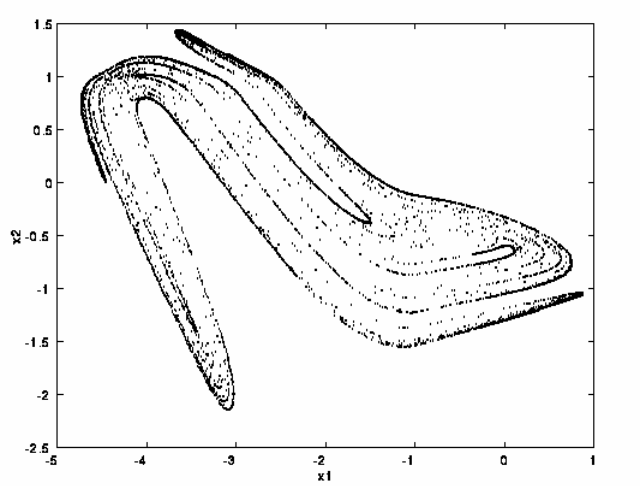

Fig.7 The Poincare map extracted from the strange attractor in Fig.5(c) is called the "Lady's shoe attractor" in view of its striking resemblance to a high-heel lady's pump.

A discrete op-amp circuit[3] for simulating Eq.(8.7) is shown in Fig.8. The experimentally observed strange attractor corresponding to Fig.5(c) is shown in Fig.9(a). The corresponding Poincare map obtained experimentally by "blanking" out the oscilloscope beam except at regular intervals of T is shown in Fig.9(b). It is sometimes instructive to interpret such Poincare maps as "strobing" the strange attractor by a stroboscope.

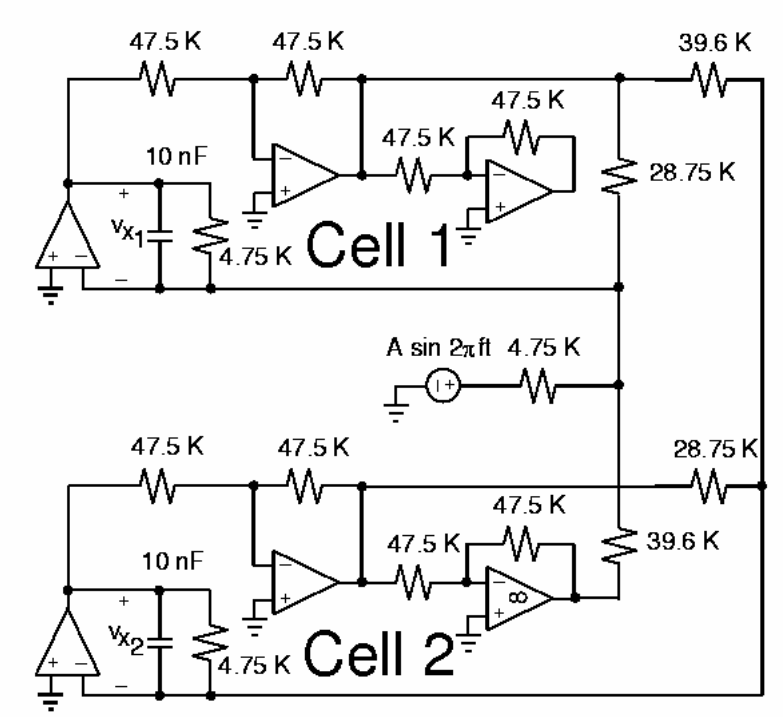

Fig. 8 A two-cell CNN circuit driven by a sinusoidal signal.

[3] F. Zou, G. Seiler, A.J. Schuler, B. Eppinger and J.A. Nossek, "Experimental confirmation of the lady's shoe attractor", *IEEE Trans. on Circuits and Systems*, vol.39, no.10, pp.844-846, 1992.

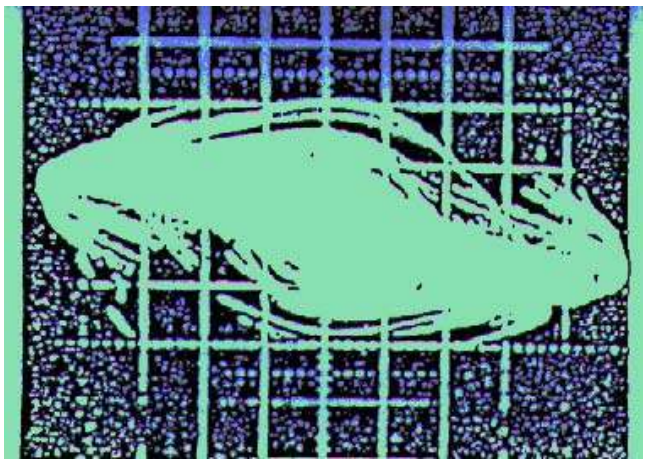

(a)

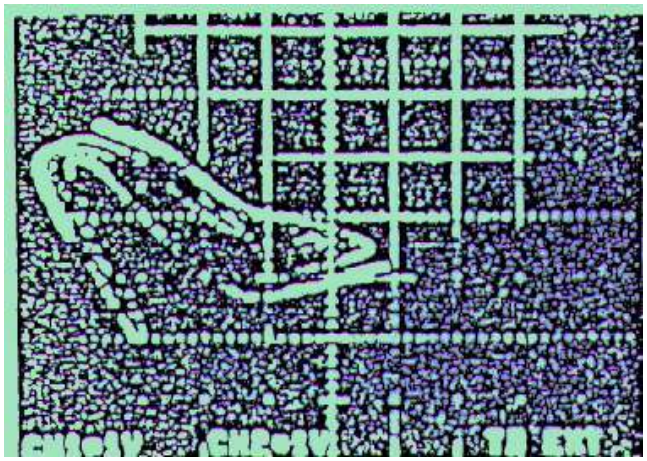

(b)

Fig.9 (a) Strange attractor obtained experimentally from the circuit in Fig.8. (b) The "lady's shoe" Poincare map extracted experimentally from the attractor in (a).

8.4. Symmetric A-template Implies Complete Stability

The preceding examples show that even CNN's with only two cells may not be completely stable. Fortunately, the following theorem guarantees the complete stability of an important subclass of CNN's. To simplify the proof of this theorem, we will assume that the nonlinear function $y_{ij} = f(x_{ij})$ is *bounded*, *differentiable* and has *positive slope* everywhere. There is little loss of generality in this assumption since our original piecewise-linear function can be approximated arbitrarily closely by such a smooth function. In fact, any physical realization of $f(x_{ij})$ will be "smooth" rather than piece-wise-linear so that this assumption is actually more consistent with reality.

Complete Stability ***Theorem 1***

Any MxN space-invariant CNN of arbitrary neighborhood size with *constant inputs* and *constant threshold* is *completely stable* if the following three hypotheses are satisfied:

1. The A template is symmetric:

$$A(i,j;k,l)=A(k,l;i,j) \tag{8.8}$$

2. The nonlinear function $y_{ij} = f(x_{ij})$ is *differentiable*, *bounded*, and

$$f'(x_{ij}) > 0 \text{ , for all } -\infty < x_{ij} < \infty \tag{8.9}$$

3. All equilibrium points are *isolated*.[4]

Proof. Consider the CNN state equation (2.8) from Chapter 2 for *constant* input **u** and threshold **z**:

$$\dot{\mathbf{x}} = -\mathbf{x} + \hat{A}\,\mathbf{y} + \hat{B}\,\mathbf{u} + \mathbf{z} \tag{8.10}$$

$$y_i = f(x_i), \qquad i = 1,2, \ldots, n = MN \tag{8.11}$$

Here, $\hat{A}$ and $\hat{B}$ are nxn matrices whose nonzero entries are the synaptic weights A(i,j;k,l) and B(i,j;k,l), respectively. Observe that hypothesis (8) and space invariance imply that

$$\hat{A} = \hat{A}^{T} \tag{8.12}$$

independent of the packing scheme.

Now, hypothesis (9) implies that f(•) is a one-to-one (injective) function and therefore has an *inverse* function

$$x_i = f^{-1}(y_i) \tag{8.13}$$

defined for all y_i over the range of $f(x_i)$, $x_i \in (-\infty, \infty)$. Define the *scalar function*

$$V(\mathbf{x}) = -\frac{1}{2}\mathbf{y}^{T}\hat{A}\mathbf{y} + \sum_{i=1}^{n}\left[\int_{\theta}^{y_i} f^{-1}(v)dv\right] - \mathbf{y}^{T}\hat{B}\mathbf{u} - \mathbf{y}^{T}\mathbf{z} \tag{8.14}$$

where θ is any number such that $f(-\infty)<\theta<f(\infty)$. [5]

A scalar function V(**x**) is called a *Lyapunov function* if its time derivative along any trajectory is non-positive, i.e.,

[4] An equilibrium point $\mathbf{x_Q}$ of $\dot{\mathbf{x}} = \mathbf{f(x)}$ is said to be *isolated* if, and only if, there are no other equilibrium points in a sufficiently small neighborhood of $\mathbf{x_Q}$.

[5] In the nonlinearity f we have been using, we can choose θ=0, since $f(-\infty) = -1$, $f(\infty) = 1$. For the sake of generality, the hypothesis on f does not require that the values of f lie between -1 and 1.

$$\dot{V}(\mathbf{x}) \triangleq \frac{dV(\mathbf{x})}{dt} = \sum_{i=1}^{n} \frac{\partial V(\mathbf{x})}{\partial x_i} \dot{x}_i \leq 0.$$

Our first goal is to prove that Eq.(8.14) defines a Lyapunov function.

Observe that the right-hand side of Eq.(8.14) is a *scalar* function of $\mathbf{x} = [x_1, x_2, \ldots, x_n]^T$ since $y_i = f(x_i)$ via Eq.(8.11). Taking the *time* derivative of both sides of Eq.(8.14) we obtain

$$\dot{V}(\mathbf{x}) = -\frac{1}{2}(\dot{\mathbf{y}}^T \hat{A}\mathbf{y} + \mathbf{y}^T \hat{A}\dot{\mathbf{y}}) + (\sum_{i=1}^{n} f^{-1}(y_i).\dot{y}_i) - \dot{\mathbf{y}}^T \hat{B}\mathbf{u} - \dot{\mathbf{y}}^T \mathbf{z} \tag{8.15}$$

Now since $\mathbf{y}^T \hat{A}\, \dot{\mathbf{y}}$ is a scalar and $\hat{A} = \hat{A}^T$ in view of Eq.(8.12), we can write

$$\mathbf{y}^T \hat{A}\, \dot{\mathbf{y}} = (\mathbf{y}^T \hat{A}\, \dot{\mathbf{y}})^T = \dot{\mathbf{y}}^T \hat{A}^T \mathbf{y} = \dot{\mathbf{y}}^T \hat{A}\, \mathbf{y} \tag{8.16}$$

Substituting Eqs.(8.13) and (8.16) into Eq.(8.15) and making use of Eq.(8.10), we obtain

$$\begin{aligned} \dot{V}(\mathbf{x}) &= -\dot{\mathbf{y}}^T \hat{A}\mathbf{y} + \sum_{i=1}^{n} x_i \dot{y}_i - \dot{\mathbf{y}}^T \hat{B}\, \mathbf{u} - \dot{\mathbf{y}}^T \mathbf{z} \\ &= -\dot{\mathbf{y}}^T (\hat{A}\mathbf{y} + \hat{B}\, \mathbf{u} - \mathbf{x} + \mathbf{z}) \\ &= -\dot{\mathbf{y}}^T \dot{\mathbf{x}} \end{aligned} \tag{8.17}$$

Observe next that

$$\dot{\mathbf{y}} = \begin{bmatrix} \frac{dy_1}{dt} \\ \frac{dy_2}{dt} \\ \cdot \\ \cdot \\ \cdot \\ \frac{dy_n}{dt} \end{bmatrix} = \underbrace{\begin{bmatrix} f'(x_1) & & & & \\ & f'(x_2) & & & \\ & & \cdot & & \\ & & & \cdot & \\ & & & & f'(x_n) \end{bmatrix}}_{\mathbf{Df}(\mathbf{x})} \begin{bmatrix} \dot{x}_1 \\ \dot{x}_2 \\ \cdot \\ \cdot \\ \dot{x}_n \end{bmatrix} = \mathbf{Df}(\mathbf{x})\dot{\mathbf{x}} \tag{8.18}$$

Substituting Eq.(8.18) into Eq.(8.17) and noting that $\mathbf{Df}(\mathbf{x})$ is symmetric, we obtain:

$$\begin{aligned} \dot{V}(\mathbf{x}) &= -[\mathbf{Df}(\mathbf{x})\, \dot{\mathbf{x}}]^T \dot{\mathbf{x}} \\ &= -(\dot{\mathbf{x}}^T \mathbf{Df}(\mathbf{x})\, \dot{\mathbf{x}}) \\ &= -\sum_{i=1}^{n} f'(x_i)\dot{x}_i^2 \leq 0 \end{aligned} \tag{8.19}$$

Hence, $V(\mathbf{x})$ in Eq.(8.14) is a Lyapunov function. Let M denote the set of all points $\mathbf{x} \in \mathbf{R}^n$ where $\dot{V}(\mathbf{x}) = 0$, i.e.,

$$M=\{\mathbf{x}:\ \dot{V}(\mathbf{x}) = 0\} \tag{8.20}$$

Since $f'(x_i) > 0$ (hypothesis 2), Eq.(8.19) implies $\dot{\mathbf{V}}(\mathbf{x}) = 0$ if, and only if, $\dot{\mathbf{x}}_i = 0$, i = 1,2, ..., n. It follows that M in Eq.(8.20) consists of the set of all equilibrium points of Eq.(8.10). Hence,

$$\boxed{\dot{V}\ (\mathbf{x}) < 0 \qquad \text{for all } \mathbf{x} \in \mathbf{R}^n \text{ except at equilibrium points}} \tag{8.21}$$

Now since **x**(t) is *bounded* in view of *Theorem 2* from Chapter 2, we can apply *LaSalle invariant principle*[6] to conclude that *all trajectories* of Eq.(10) must converge to the *invariant set*[7] M of equilibrium points.

Now since all equilibrium points of Eq.(10) are isolated (hypothesis 3), it follows that all trajectories of Eq.(10) must converge to an equilibrium point.

Remarks

1. If the equilibrium points in M are not isolated[8], then our theorem can be relaxed to assert only that all trajectories must converge to the set M of equilibrium points. Strictly speaking, this assertion does not imply that every trajectory will converge to an equilibrium point since there exists (admittedly highly pathological and rare) situations where every trajectory will approach M at an arbitrarily small rate so that $\dot{\mathbf{x}}_i \to 0$ and yet the trajectory never converges to any particular equilibrium point.

2. To visualize the geometrical ideas behind the above proof, consider the hypothetical surface $V(x_1, x_2)$ shown in Fig.10. Notice that this surface has five local minima $\{Q_1, Q_3, Q_5, Q_7, Q_9\}$. Imagine the inside of the surface V as the surface of a rugged narrow mountain crevice and a small ball is coasting down the surface. One such hypothetical trajectory Γ representing the "track" made by the ball is shown in Fig.10. Notice that due to gravity, a ball originating from any point other than an extremum point must keep falling down along the steep slope until it settles down at a local minimum; i.e.,

$$\dot{V}(x_1, x_2) = \frac{d}{dt} V(x_1(t), x_2(t)) < 0 \tag{8.22}$$

for all $(x_1, x_2) \neq (x_1(Q_i), x_2(Q_i))$.

---

[6] J.P. LaSalle, " An invariant principle in the theory of stability," in J.K. Hale and J.P. Salle, Editors, *Differential Equations and Dynamical Systems*, Academic Press 1967.

[7] A set $M \subset R^n$ is called an *invariant set* of Eq.(8.10), if any trajectory starting from a point $x_0 \in M$ at t=0 remains in M for all t>0. Since M in this case contains only equilibrium points, it is clearly an invariant set.

[8] We have already encountered such a situation in Fig.3(c) of Chapter 6.

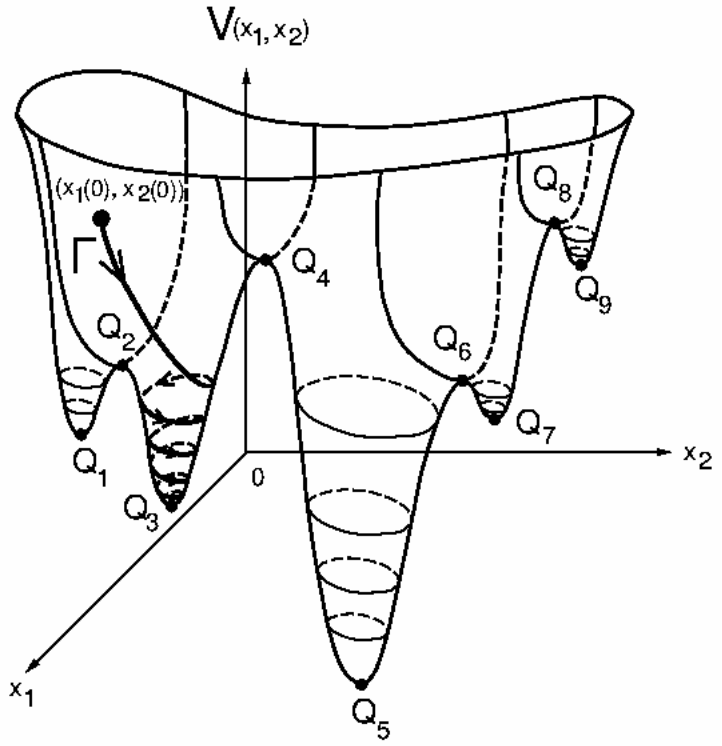

Fig.10 A hypothetical Lyapunov function $V(x_1, x_2)$ with five local extrema Q_1, Q_3, Q_5, Q_7, Q_9, *and a hypothetical trajectory* Γ *converging toward the local minimum* Q_3.

An n-dimensional *scalar* function

$$V(x_1, x_2, ..., x_n) : R^n \rightarrow R^1 \tag{8.23}$$

is called a *Lyapunov function* associated with an *autonomous* system of differential equations

$$\dot{\mathbf{x}}_i = f_i(x_1, x_2, ..., x_n), \quad i = 1, 2, ..., n \tag{8.24}$$

if, and only if , corresponding to *any* trajectory

$$(x_1, x_2, ..., x_n) = (\gamma_1(t), \gamma_2(t), ..., \gamma_n(t)) \tag{8.25}$$

of Eq.(8.24), the corresponding scalar function of time

$$V(t) \triangleq V(\gamma_1(t), \gamma_2(t), ..., \gamma_n(t)) \tag{8.26}$$

decreases monotonically with time, i.e., $\dot{V}(t) \leq 0$. In particular, if $\dot{V}(t) = 0$ *only* at equilibrium points, then it follows that all trajectories must land at an equilibrium point Q_i and the set $\mathcal{B}(Q_i)$ of all initial conditions such that corresponding trajectories converge to Q_i is the *basin of attraction* of Q_i. It follows from the above geometrical insights that one method to prove Eq.(8.24) is completely stable is to find a scalar function $V(x_1, x_2,$

..., x_n) which possesses the above properties.[9] Unfortunately, no systematic procedure is presently available for finding such a scalar function, partly because solutions of most *nonlinear* systems of differential equations, such as Eq.(8.24), can *not* be found by analytical methods.

Now that the degree of difficulty for proving complete stability of Eq.(8.24) is understood, the reader would no doubt appreciate how lucky we are in being able to invent the scalar function V(**x**) in Eq.(8.14) and prove that it qualifies as a Lyapunov function.

8.5. Positive and Sign-Symmetric A-template Implies Complete Stability

In this section we will present another complete stability criterion which depends only on the "sign" , and *not* the "value", of the elements of the A-template.

Definition 1: Sign symmetric A-template

Let A_{180^o} denote the template obtained by rotating an A-template by 180^o with respect to the center of the template. Let a_{ij} and a'_{ij} denote the corresponding ij-th elements of A and A_{180^o}. We say a (2r+1)x(2r+1) A-template, where r is the radius of the sphere of influence $S_r(ij)$, is *sign symmetric* if, and only if, a_{ij} and a'_{ij} are *both positive*, *both negative*, or *both zero*, for all i,j = 1, 2, ... , 2r+1.

The above definition is equivalent to the condition that a_{ij} and $a_{-i,-j}$ are *both positive*, or *both negative*, or *both zero*, for all $(i,j)\neq(0,0)$, where the double subscripts correspond to a Cartesian coordinate system whose origin is located at the center of the template. As an illustrative example, consider the 5x5 A-template shown in Fig.11(a). To determine whether this template is *sign symmetric*, we first rotate "A" by 180^o (always with respect to the center of the template) to obtain the associated A_{180^o} -template shown in Fig.11(b). We then construct the corresponding "sign" template, denoted by sgn[A] and sgn[A_{180^o}], respectively, by assigning the symbol +, -, or 0 to each entry a_{ij} where a_{ij} >0, a_{ij} <0 and a_{ij} =0 in A and A_{180^o}, respectively.

A=

-2	0	7	-5	0
1	6	0	-2	-6
0	2	4	3	0
-4	-3	0	6	2
0	-6	8	0	-3

A_{180^o} =

-3	0	8	-6	0
2	6	0	-3	-4
0	3	4	2	0
-6	-2	0	6	1
0	-5	7	0	-2

[9] This is, in fact, the *only general* tool currently available to prove complete stability of Eq.(24).

$$\text{sgn}[A] = \text{sgn}[A_{180^o}] =$$

-	0	+	-	0
+	+	0	-	-
0	+	+	+	0
-	-	0	+	+
0	-	+	0	-

Fig. 11 (a) A non-symmetric 5x5 A-template ($A \neq A^T$). (b) A_{180^o} obtained by rotating the A-template 180^o with respect to the center of the template. (c) The "sign" of corresponding coefficients of A and A_{180^o} are identical as depicted in this "sign" template sgn[A] whose entries consist of +, -, and 0's.

Then the A-template is sign symmetric if, and only if,

$$\text{sgn}[A] = \text{sgn}[A_{180^o}] \tag{8.27}$$

Since Eq.(8.27) is satisfied as shown in Fig.11(c), we conclude that the A-template in Fig.11 is sign symmetric. Observe that this template is not symmetric with respect to the center, i.e., a sign-symmetric A-template is, in general, not symmetric, but a symmetric A-template is always sign symmetric.

Definition 2. Synaptic weight conditions

Each of the following conditions concerning the relative signs of the *synaptic weights* a_{ij} of a (2r+1)x(2r+1) A-template is called a *synaptic weight condition*:

A=

$a_{-r,-r}$	.	.	.	$a_{-r,-1}$	$a_{-r,0}$	$a_{-r,1}$	.	.	.	$a_{-r,r}$
$a_{-r+1,-r}$	.	.	.	$a_{-r+1,-1}$	$a_{-r+1,0}$	$a_{-r+1,1}$				$a_{-r+1,r}$
.										
.										
.										
$a_{0,-r}$	.	.	.	$a_{0,-1}$	$a_{0,0}$	$a_{0,1}$	.	.	.	$a_{0,r}$
.										
.										
.										
$a_{r-1,-r}$	.	.	.	$a_{r-1,-1}$	$a_{r-1,0}$	$a_{r-1,1}$	.	.	.	$a_{r-1,r}$
$a_{r,-r}$	.	.	.	$a_{r,-1}$	$a_{r,0}$	$a_{r,1}$	.	.	.	$a_{r,r}$

Synaptic weight condition 1:

$$a_{kl} \geq 0 \quad \text{for all } (k, l) \neq (0, 0) \tag{8.28}$$

Synaptic weight condition 2:

$a_{kl} \geq 0$ for all $(k, l) \neq (0, 0)$ and "even" k.
$a_{kl} \leq 0$ for all "odd" k (8.29)

Synaptic weight condition 3:

$a_{kl} \geq 0$ for all $(k, l) \neq (0, 0)$ and "even" l.
$a_{kl} \leq 0$ for all "odd" l (8.30)

Synaptic weight condition 4:

$a_{kl} \geq 0$ for all $(k, l) \neq (0, 0)$ and "even" (k+l).
$a_{kl} \leq 0$ for all "odd" (k+l) (8.31)

We are now ready to state our next theorem.

Complete Stability ***Theorem 2***[10]

An MxN CNN with a (2r+1)x(2r+1) A-template is *completely stable*, for arbitrary *B-template* and arbitrary *threshold* z, if the following three conditions are satisfied:

1. The A-template is *sign symmetric*.

2. The template satisfies any one of the four *synaptic weight conditions*.

3. All the equilibrium points are isolated.

The proof of a special case of this theorem will be given in the next section.

Remark

Note that the synaptic weight condition 1 corresponds to an A-template with non-negative coefficients (except possibly the center). Hence the title of this section is a *Corollary* of the above theorem.

Corollary to Complete Stability ***Theorem 2***

An MxN CNN with a 3x3 A-template, for arbitrary *B-template* and arbitrary *threshold z,* is *completely stable* if the following three conditions are satisfied:

1. The A-template is *sign symmetric*.

2. The A-template possesses *any one* of the six synaptic weight patterns shown in Fig.12.

[10] To be more precise, for theorems 2-4 (and the corollaries to these theorems) in this section, we should add that the complete stability property, unlike in theorem 1, apply to all initial conditions *except* for a set of measure zero. For example, there may exist (possibly rare) such completely stable CNN's where there is an *unstable* limit cycle.

⊕	⊖	⊕
⊖	5	⊖
⊕	⊖	⊕

synaptic weight pattern 1

⊖	⊕	⊖
⊖	5	⊖
⊖	⊕	⊖

synaptic weight pattern 2

⊖	⊖	⊖
⊕	5	⊕
⊖	⊖	⊖

synaptic weight pattern 3

⊖	0	⊕
0	5	0
⊕	0	⊖

synaptic weight pattern 4

⊕	0	⊖
0	5	0
⊖	0	⊕

synaptic weight pattern 5

⊕	⊕	⊕
⊕	5	⊕
⊕	⊕	⊕

synaptic weight pattern 6

Fig.12. Six synaptic weight patterns which satisfy condition 2 of the Complete Stability Theorem 2.

where

0	denotes a "zero" synaptic weight
⊕	denotes a "positive" *or* "zero" synaptic weight
⊖	denotes a "negative" *or* "zero" synaptic weight
5	may assume *any* value.

3. All the equilibrium points are isolated.

Proof. This corollary follows directly from the above theorem since each of the synaptic weight pattern 1-3, and six satisfies one of the four synaptic weight conditions in (28)-(31).

Synaptic patterns 4 and 5 are trickier and we give the following sketch of the argument. If we rotate synaptic pattern 4 by 45^{o}, counterclockwise, we obtain the pattern

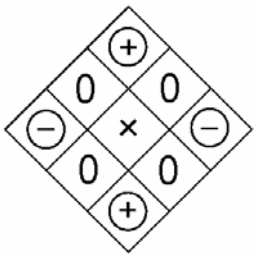

Looking at the nonzero entries, the center element is connected only to the top, down, left and right neighbors. It can be shown that this is similar to the template

0	⊕	0
⊖	5	⊖
0	⊕	0

which belongs to the class of synaptic pattern 2. The same can be said by rotating synaptic pattern 5 by 45^o clockwise.

Thus the stability of synaptic patterns 4 and 5 can be deduced from the stability of synaptic pattern 2.

To illustrate the properties of the synaptic weight patterns in Fig.12, consider the following set of 12 hypothetical templates:

$A_1 = \begin{bmatrix} 0 & -2 & 0 \\ 2 & 7 & 4 \\ 0 & 0 & 0 \end{bmatrix}$, $A_2 = \begin{bmatrix} 0 & -2 & 7 \\ -4 & 7 & -3 \\ 7 & -1 & 0 \end{bmatrix}$, $A_3 = \begin{bmatrix} 0 & 0 & 0 \\ -2 & 9 & -1 \\ 0 & 0 & 0 \end{bmatrix}$

$A_4 = \begin{bmatrix} 7 & 0 & -1 \\ 0 & 8 & 0 \\ 0 & 0 & 0 \end{bmatrix}$, $A_5 = \begin{bmatrix} -7 & 0 & 0 \\ 0 & 2 & 0 \\ 2 & 0 & -6 \end{bmatrix}$, $A_6 = \begin{bmatrix} 0 & 1 & 2 \\ -3 & 4 & -5 \\ 0 & 0 & 0 \end{bmatrix}$

$A_7 = \begin{bmatrix} 0 & 0 & 1 \\ 2 & 3 & 4 \\ 5 & 6 & 0 \end{bmatrix}$, $A_8 = \begin{bmatrix} 0 & 0 & 0 \\ -1 & -2 & -3 \\ 0 & -5 & 0 \end{bmatrix}$, $A_9 = \begin{bmatrix} -1 & -2 & -3 \\ 4 & 5 & 0 \\ 0 & -7 & 0 \end{bmatrix}$

$A_{10} = \begin{bmatrix} -1 & 0 & -2 \\ 0 & 7 & 0 \\ -3 & 0 & 0 \end{bmatrix}$, $A_{11} = \begin{bmatrix} 1 & -4 & 5 \\ 7 & 0 & 8 \\ 6 & 2 & 0 \end{bmatrix}$, $A_{12} = \begin{bmatrix} -2 & -1 & 4 \\ 2 & 3 & 1 \\ 1 & -5 & -7 \end{bmatrix}$

The following table summarizes the properties of these templates:

Template	Is template A_i sign-symmetric?	Synaptic weight pattern possessed by template A_I
A_1	NO	3
A_2	YES	1
A_3	YES	1, 2
A_4	NO	5
A_5	NO	4
A_6	NO	NONE
A_7	NO	6
A_8	NO	1
A_9	NO	3
A_{10}	NO	2
A_{11}	NO	NONE
A_{12}	YES	NONE

Observe that since none of the above 12 templates are symmetric, we cannot make use of the *Complete Stability Theorem 1*. However, applying the *Corollary to Complete Stability Theorem 2*, we can assert that templates A_2 and A_3 are completely stable.

8.6. Positive and Cell-linking A-template Implies Complete Stability

In this section we will present yet another complete stability criterion, which substitutes the "sign symmetry" condition from Theorem 2 by a certain condition on the signal flow graph $\mathcal{G}_A$(MxN) associated with an MxN CNN, where $\mathcal{G}_A$(MxN) denotes a *directed* graph obtained by associating *each cell* C(i,j) of the CNN with a *node* (i,j) and where *each* node is connected to its neighbors via the signal flow graph $\mathcal{G}_A$ associated with the A-template defined in Fig.17 of Chapter 2.

Definition 3. CNN Signal flow graph $\mathcal{G}_A$(MxN)

For each MxN CNN, we construct a *directed graph* $\mathcal{G}_A$(MxN) corresponding to an A-template as follows:

1. Draw the signal flow graph $\mathcal{G}_A$ associated with the A-template. For each non-zero and non-central synaptic weight $a_{kl}\neq 0$ ($k\neq i$, $l\neq j$) in A, draw a *directed* branch *from* node (k,l) *to* the center node (i,j), and a *similarly-directed* branch from the center node (i,j) to the *reflected* node $(\bar{k}, \bar{l})$; i.e., node $(\bar{k}, \bar{l})$ is related to node (k,l) by a 180^o rotation with respect to the center node (i,j).[11] See Figs.13(a) and 13(b) for an example.

[11] In this section, it is useful to think of each directed branch as a *one-way* street and a node as an intersection between two or more one-way streets. Hence for each nonzero entry in A ($a_{kl} \neq 0$), there are two connecting one-way streets in the same direction which allows one to travel from node (k,l) to node $(\bar{k}, \bar{l})$. Two or more such branches in a directed graph are said to be *similarly directed*.

As an example, the signal flow graph $\mathcal{G}_A$ associated with the A-template in Fig.13(a) is shown in Fig.13(b). Observe that $\mathcal{G}_A$ has six directed branches (not counting the self loop) since there are only three non-zero non-central entries in the A-template; namely, $a_{-1,-1} = -2.6$, $a_{-1,0} = 1.5$ and $a_{1,1} = 3.2$. Observe that for each *zero* entry ($a_{k,l} = 0$, $k\neq l$) in the A-template, the corresponding node (k,l) in $\mathcal{G}_A$ has no branches attached to it. Observe also that the "sign" of $a_{kl} \neq 0$ is *irrelevant* in so far as the *direction* of the associated branch is concerned, which always goes from node (k,l) to the center node (i,j), and its reflected "twin" branch always goes from the center node (i,j) to node $(\bar{k}, \bar{l})$.

In the signal flow graph $\mathcal{G}_A$ shown in Fig.13(b), we also write the synaptic weight a_{kl} next to the pair of directed branches associated with each entry of the A-template where $a_{kl} \neq 0$. For completeness, we also draw a *self-loop* at node (i,j) with the *self-feedback* synaptic weight $a_{ij} = 4.7$ written next to it. For the purpose of this section, however, both the synaptic weights and the self-loop are irrelevant to the following complete stability theorem and will therefore be deleted from $\mathcal{G}_A$.

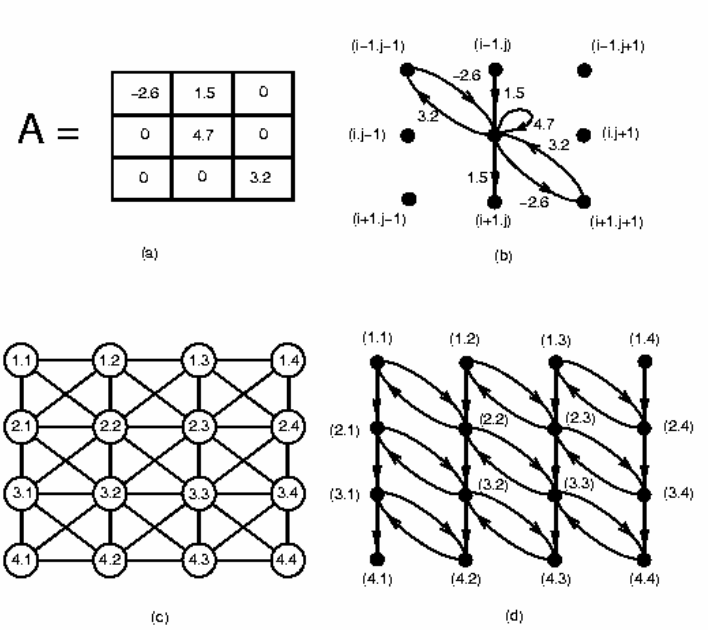

Fig.13. Steps for constructing the signal flow graph $\mathcal{G}_A$(MxN) *of an MxN CNN: (a) Specify the A-template (b) Draw the signal flow graph* $\mathcal{G}_A$ *associated with the A-template. Note that for each non-zero synaptic weight* $a_{kl} \neq 0$, $k \neq l$, *there correspond two branches in* $\mathcal{G}_A$ *. (c) a 4x4 (M=N=4) CNN. (d) The reduced signal flow graph* $\mathcal{G}_A$(4x4) *associated with the A-template.*

2. To each cell C(k,l) in an MxN CNN, draw a corresponding node (k,l), k=1,2 ..., M, l=1,2, ..., N (see Figs.13(c) and 13(d) for a 4x4 CNN).

3. Duplicate the signal flow graph $\mathcal{G}_A$ (delete the coefficients a_{kl} and the self-loop) from *step 1* at each node (k,l) from *step 2*. All branches connected to "virtual" boundary nodes are deleted. The resulting directed graph is called the reduced CNN *signal flow graph* $\mathcal{G}_A$(MxN). For the 4x4 CNN shown in Fig.13(c), we obtain the 16-node directed graph $\mathcal{G}_A$(4x4) shown in Fig.13(d).

Definition 4. Cell-linking CNN

Let $\mathcal{G}_A$(MxN) be the signal flow graph of an MxN CNN associated with an A-template. Then the CNN is said to be *cell-linking* if, and only if, for *every* two distinct nodes (k_1, l_1) and (k_2, l_2) in $\mathcal{G}_A$(MxN), there is a *similarly directed path*[12] in $\mathcal{G}_A$(MxN) from node (k_1, l_1) to node (k_2, l_2), *and* a *similarly directed return path* from node (k_2, l_2) to node (k_1, l_1).

For example, the 4x4 CNN shown in Fig.13(c) is *not* cell-linking because there is at least one pair of nodes (e.g., from node (2, 1) to node (1,1)) where no similarly-directed path exists. On the other hand, the 4x5 CNN shown in Fig.14 is cell-linking as

[12] A similarly-directed path from node (k_1, l_1) to node (k_2, l_2) is defined as a sequence of *directed* branches (one-way streets) which allows one to travel from an *initial* node (k_1, l_1) to a destination node (k_2, l_2).

the reader can verify that there is a similarly-directed path from any node (k_1, l_1) in the signal flow graph $\mathcal{G}_A$(4x5) to any other node (k_2, l_2). For example, to go from node (2,2) to node (3,4), we would travel along the similarly-directed path (2,2) $\rightarrow$(3,2) $\rightarrow$(2,3) $\rightarrow$(3,3) $\rightarrow$(4,3) $\rightarrow$(3,4).

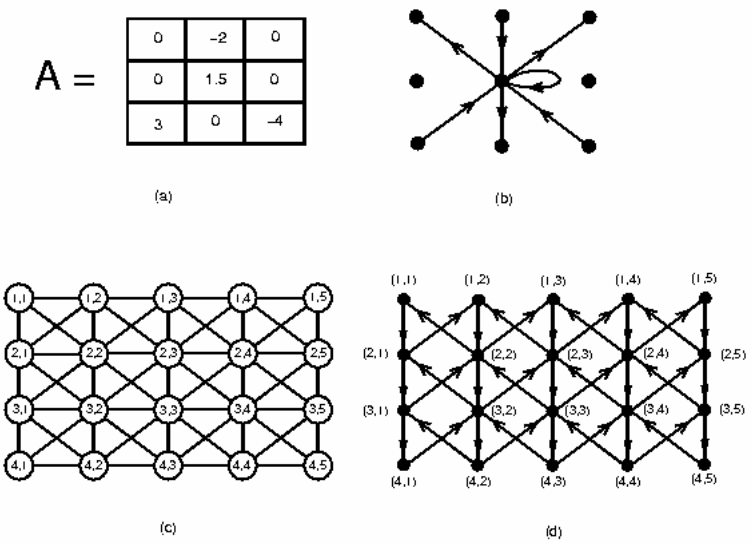

Fig.14. Example of a 4x5 cell-linking CNN

Observe that before one can certify that a particular CNN is cell-linking, definition 4 requires that one must examine *all possible combinations* of *initial* and *terminal* node pairs and in each case produce a similarly-directed path. This would be a tedious task unless a computer program is written to do the checking. Fortunately, the following 3 *cell-linking tests* can be used to certify quickly, often by inspection, a large class of NxN CNN′s to be cell-linking.

Cell-linking test 1

An NxN CNN, where N is an odd integer, is *cell-linking* if, and only if, there is a *similarly-directed path* from the *center node*[13] of the associated signal flow graph $\mathcal{G}_A$(NxN) *to every other nodes* of $\mathcal{G}_A$(NxN).

Example 1.

Consider the 3x3 CNN obtained by deleting row 4 and column 4 from the 4x4 CNN in Fig. 13(c). The corresponding signal flow graph $\mathcal{G}_A$ (3x3) is obtained by deleting all nodes, and the branches attached to them, from the last row and the last column in Fig.13(d). In this case, node (2,2) is the *center node* of the associated signal flow graph $\mathcal{G}_A$ (3x3). Since there is no *similarly-directed* path going from node (2,2) to node (1,3) in $\mathcal{G}_A$(3x3), we conclude that this 3x3 CNN is *not* cell-linking.

[13] Since N is an odd integer, the geometric center of $\mathcal{G}_A$(NxN) is a node of $\mathcal{G}_A$(NxN).

Example 2.

Consider the 3x3 CNN obtained by deleting row 4 and columns 4, 5 from the 4x5 CNN in Fig.14(c). The corresponding signal flow graph $\mathcal{G}_A$ (3x3) is obtained by deleting all nodes, and the branches attached to them, from the last row and the last two columns in Fig.14(d). In this case, node (2,2) is the *center node* of the associated signal flow graph $\mathcal{G}_A$ (3x3). Observe that there is a *similarly-directed path* from node (2,2) to every other nodes of $\mathcal{G}_A$(3x3):

(2,2)→ (1,1),
(2,2) → (1,3) → (2,3) → (1,2),
(2,2) → (1,3),
(2,2) → (3,2) → (2,1),
(2,2) → (1,3) → (2,3),
(2,2) → (3,2) → (2,1) → (3,1),
(2,2) → (3,2),
(2,2) → (3,2) → (2,3) → (3,3).

It follows from the *cell-linking test 1* that this 3x3 CNN is cell-linking.

Proof of cell-linking test 1:

The proof of this test follows from the proof of the following cell-linking test 2, since the center cell is rotationally symmetric with respect to itself.

Definition 5: Symmetric node-pair

If "a" is a node of the signal flow graph $\mathcal{G}_A$(MxN) let a* denote the corresponding node which is 180^o rotationally symmetric (about the center) with respect to a.

Lemma 1:

There is a similarly-directed path from node a to node b in $\mathcal{G}_A$ if, and only if, there is a similarly-directed path from node b* to node a*.

Proof:

We will prove this Lemma by *mathematical induction* on the length n of the path as follows:

n=1: if there is a branch from node a to b then there is a branch from b* to a* in view of the space-invariance of the templates, as shown in Fig.15.

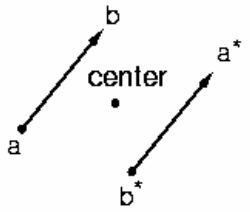

Fig.15 A branch from a to b implies that a branch exists from b to a*, and vice versa.*

A directed path of length n=k+1 from a to b contains a path of length k from a to c and a branch from c to b. By the induction hypothesis, there is a path of length k from c* to a* and a branch from b* to c*. So there is a path of length k+1 from b* to a*. See Fig.16.

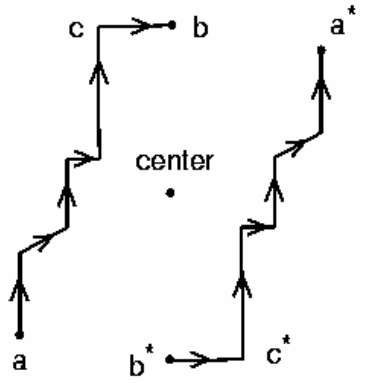

Fig.16 A directed path from a to b implies that a directed path exists from b to a*, and vice versa.*

Cell-linking test 2.

An MxN CNN is cell-linking if, and only if, there is a pair of *rotationally symmetric* nodes[14] (k,l) and $(\bar{k}, \bar{l})$ such that there is a similarly-directed path from node (k,l) to *every other nodes* of $\mathcal{G}_A$(MxN), *and* a *similarly-directed path* from node $(\bar{k}, \bar{l})$ to *every other nodes* of $\mathcal{G}_A$(MxN) .

Example 3:

Consider the 4x4 CNN shown in Fig.13(c) and its associated signal flow graph $\mathcal{G}_A$(4x4) in Fig.13(d). Observe that *for every pair* of rotationally symmetric nodes (k,l) and $(\bar{k}, \bar{l})$, of which there are many (e.g., (1,1) and (4,4), (3,2) and (2,3), (2,1) and (3,4), etc.), in $\mathcal{G}_A$(4x4), we cannot find a pair (k,l) and $(\bar{k}, \bar{l})$ such that there exists a *similarly-directed* path from node (k,l) (resp. $(\bar{k}, \bar{l})$) to every other nodes of $\mathcal{G}_A$(4x4). It follows from *cell-linking test 2* that the 4x4 CNN of Fig.13 is *not* cell-linking.

Example 4:

Consider the 4x4 CNN obtained by deleting column 5 from the 4x5 CNN in Fig.14(c). The corresponding signal flow graph $\mathcal{G}_A$(4x4) is obtained by deleting all nodes, and the branches attached to them, from the last column in Fig.14(d). Consider the rotationally-symmetric pairs of nodes (1,1) and (4,4). Observe that there is a *similarly-directed* path from node (1,1) to *every other nodes* of $\mathcal{G}_A$(4x4):

(1,1)→ (2,1),
(1,1) → (2,1) → (3,1),

[14] Two nodes (k,l) and $(\bar{k}, \bar{l})$ are said to be rotationally symmetric if, and only if, the position of (k,l) coincides with that of $(\bar{k}, \bar{l})$ upon rotating the CNN by 180^o about its center position.

(1,1) → (2,1) → (3,1) → (4,1),
(1,1) → (2,1) → (1,2),
(1,1) → (2,1) → (1,2) → (2,2),
(1,1) → (2,1) → (1,2) → (2,2) → (3,2),
(1,1) → (2,1) → (1,2) → (2,2) → (3,2) → (4,2),
(1,1) → (2,1) → (1,2) → (2,2) → (1,3) ,
(1,1) → (2,1) → (1,2) → (2,2) → (1,3) → (2,3),
(1,1) → (2,1) → (1,2) → (2,2) → (1,3) → (2,3) → (3,3),
(1,1) → (2,1) → (1,2) → (2,2) → (1,3) → (2,3) → (3,3) → (4,3),
(1,1) → (2,1) → (1,2) → (2,2) → (1,3) → (2,3)→ (1,4),
(1,1) → (2,1) → (1,2) → (2,2) → (1,3) → (2,3) → (1,4) → (2,4),
(1,1) → (2,1) → (1,2)→(2,2)→(1,3)→(2,3)→(1,4)→(2,4)→ (3,4),
(1,1) → (2,1) → (1,2) → (2,2) → (1,3) → (2,3) → (1,4) → (2,4)→(3,4) → (4,4).

A *similarly-directed path* can also be found from node (4,4) to every other node of $\mathcal{Y}_A$(4x4). It follows from *cell-linking test 2* that this 4x4 CNN is cell-linking.

Proof of cell-linking test 2:

If the template is cell-linking, then by definition a and a* have similarly-directed paths to every other cell. Suppose both a and a* have similarly-directed paths to every other cell. Consider cell c different from a. Then cell c* is different from a*. So there is a path from a* to c*. By Lemma 1, there is a path from c to a. Since there is a path from a to everywhere else, c has a path to everywhere else too.

Cell-linking test 3

Let C(M_1xN_1) denote any CNN subset of an MxN CNN, where M_1<M and N_1<N. Suppose N_1>1 and M_1>1. If C(M_1xN_1) is cell-linking, then so is its associated MxN CNN.

Example 5.

Consider the 4x5 CNN shown in Fig.14. Since *Example 4* shows that the 4x4 CNN subset is cell-linking, it follows from the *cell-linking test 3* that the associated 4x5 CNN is also cell-linking.

Proof of cell-linking test 3:

The proof is trivial by noting that the signal flow graph of an M_1x N_1 CNN can be obtained from the signal flow graph of an MxN CNN (M≥ M_1, N≥ N_1) by deleting some nodes and the branches connected to them. Thus a path in the smaller graph is also a valid path in the bigger graph.

We are now ready to state our next complete stability criterion.

Complete Stability ***Theorem 3****.*

An MxN CNN with a (2r+1)x(2r+1) A-template is *completely stable*, for *arbitrary B-templates* and *arbitrary threshold z*, if the following three conditions are satisfied:

1. The CNN is *cell-linking*.

2. Any one of the four *synaptic weight conditions* given by Eqs.(8.28)-(8.31).

3. All the equilibrium points are isolated.

Corollary to Complete Stability Theorem 3.

An NxN CNN with a 3x3 A-template, an *arbitrary B-template*, and an *arbitrary threshold z*, is *completely stable* if the following three conditions are satisfied:

1. The CNN is *cell-linking*.

2. The A-template possesses *any one* of the six *synaptic weight patterns* given in Fig.12.

3. All the equilibrium points are isolated.

Proof.

We will only sketch the proof of this corollary. For the proof of the complete stability theorem 3, see [15].

Let us first prove the above Corollary for the synaptic weight pattern 6. The state equation is

$$\dot{\mathbf{x}} = -\mathbf{x} + \hat{\mathbf{A}}\, f(\mathbf{x}) + \hat{\mathbf{B}}\, \mathbf{u} + \mathbf{z}$$

The Jacobian matrix of the system is

$$(-I + \hat{A}\, J)$$

where I is the identity matrix and

$$J = \begin{bmatrix} f'(x_1) & & & \\ & . & & \\ & & . & \\ & & & . \\ & & & f'(x_n) \end{bmatrix}$$

The off-diagonal elements of $\hat{\mathbf{A}}$ are the off-center elements of the A-template which are nonnegative. Cell-linking implies the *irreducibility*[16] of the matrix $\hat{\mathbf{A}}$ and hence $-I+\hat{\mathbf{A}}\, J$ is

[15] L.O. Chua and C.W. Wu, "On the universe of stable cellular neural networks," *Int. J. Circuit Theory and Applications*, vol.20, pp.497-517 (1992).

also irreducible. Since the trajectories are bounded and the equilibrium points are isolated, the conclusion follows from theorem A.1. in the Appendix of this Chapter.

By using theorem A.2. in the Appendix, the synaptic weight patterns 1-3 can be transformed into the synaptic pattern 6. Since "stability" and "irreducibility" are preserved under these transformations, the corollary is proved.

Remarks:

1. Complete stability theorem 3 can be used to prove complete stability theorem 2 since for sign-symmetric templates the signal flow graph can be decomposed into cell-linking components.

2. The "connected component detector (CCD)" template

$$A= \begin{array}{|c|c|c|} \hline 1 & 2 & -1 \\ \hline \end{array}$$

to be presented in Chapter 12 does not belong to any of the above classes.

To understand the elusiveness of this template, observe that the preceding stability criteria only make use of the "sign" of the template entries, not the actual values. In the following section, we will show that by changing the template entries of the CCD CNN by an arbitrarily small amount we can make it unstable. Consequently, any stability criterion capable of predicting the stability of the CCD template must include conditions involving the synaptic weights of the A-template.

8.7. Stability of Some Sign-antisymmetric CNN's

We have already given an intuitive reason on why the stability of the CCD CNN is very difficult to prove. Numerical simulations have shown that the trajectories associated with the CCD template always converge to an equilibrium point. But if we change the template values slightly, the system will oscillate.

In fact, computer simulations show that the parameters of the CCD template

$$A= \begin{array}{|c|c|c|} \hline 1 & 2 & -1 \\ \hline \end{array}$$

lies on a *stability boundary* in the parameter space. In particular, the slightly perturbed A-template

$$A= \begin{array}{|c|c|c|} \hline 1.01 & 2 & -1.01 \\ \hline \end{array}$$

is found to be unstable. This is illustrated in Figs.18(a) and 18(b).

These templates belongs to the class of templates

$$A = \begin{array}{|c|c|c|} \hline a^* & 2 & a \\ \hline \end{array}, \qquad B = \begin{array}{|c|c|c|} \hline 0 & 0 & 0 \\ \hline \end{array}, \qquad z = \begin{array}{|c|} \hline 0 \\ \hline \end{array}$$

[16] M.W.Hirsch, "System of differential equations that are competitive or cooperative II: Convergence almost everywhere," SIAM Math. Anal., vol.16, no.3, May 1985, pp.423-439.

When the parameters a and a* are varied, the corresponding CNN exhibit different behaviors. The a-a* parameter plane can be partitioned into eight pairs of symmetrically spread regions which exhibit the same qualitative behavior.

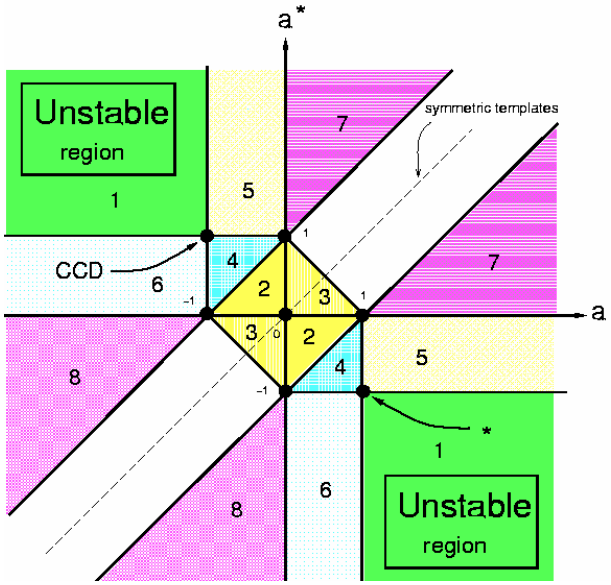

Fig. 17 Partitioning of the a-a parameter plane into 16 regions. See text for the behaviors of the CNN's in each region. The CNN at the point "*" is related to the CCD template*

$$A = \begin{bmatrix} 1 & 2 & -1 \end{bmatrix}$$

by a 180º rotation and shares the same functionality as the CCD template except that all pixels move in the other direction (see Chapter 12).

We have shown earlier that if a and a* are both positive, or both negative, then the CNN is stable (almost everywhere).

The following theorems can be proved:

Theorem 4: The CNN's in region 1 of the parameter plane in Fig 17 do *not* possess any stable equilibrium point and are therefore *not stable*.

Theorem 5: The CNN's in regions 2 and 3 of the parameter plane in Fig 17 are *completely stable* and any binary one-dimensional pattern corresponds to the output of a stable equilibrium point.

Theorem 6: The CNN's in regions 5 and 7 of the parameter plane in Fig 17 are *completely stable* and all trajectories converge to an equilibrium point with a homogeneous "white" output for all cells,

W	W	W	W	W	W	W	W	W	W

where "W" denotes a "white" output, or a homogenous "black" output for all cells:

B	B	B	B	B	B	B	B	B	B

where "B" denotes a "black" output.

Theorem 7. The CNN's in regions 6 and 8 of the parameter plane in Fig 17 are *completely stable* and all trajectories converge to an equilibrium point with an alternating "white-and-black" output

W	B	W	B	W	B	W	B	W	B

, or an alternating "black-and-white" output.

B	W	B	W	B	W	B	W	B	W

Computer simulations show that all CNN's in region 4 behave like a CCD CNN. Observe that the CCD template

$$A = \begin{array}{|c|c|c|} \hline 1 & 2 & -1 \\ \hline \end{array}$$

lies at the common corner boundary point of unstable region 1, stable regions 5 and 6 (everything converge to one of two possible patterns) and stable region 4 (CCD behavior).

Let us examine next the trajectories of the following two CNN's which lie in two different regions in the parameter space in Fig.17, but which are very close to each other:

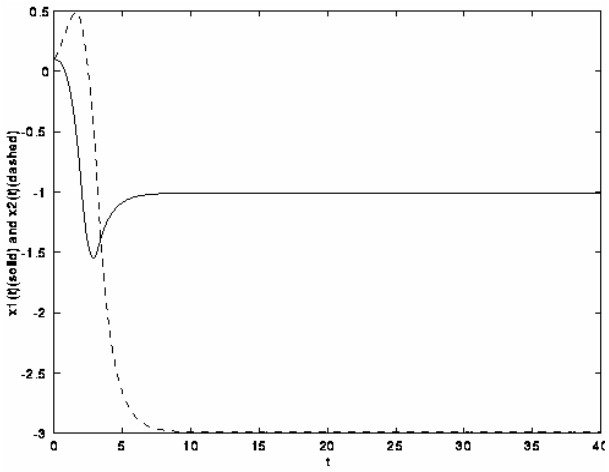

(a)

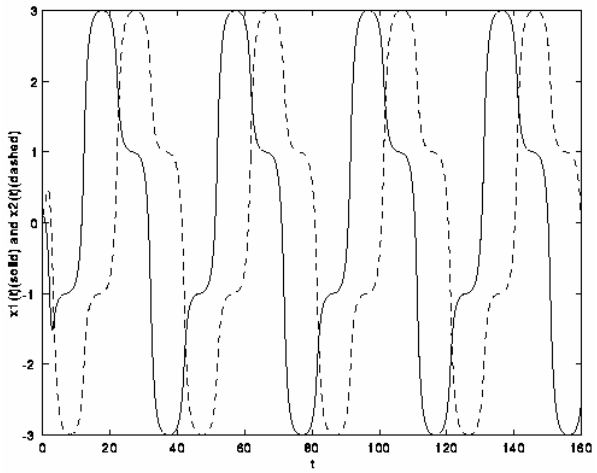

(b)

Fig.18(a) Stable output waveforms corresponding to template

A = | 0.99 | 2 | -0.99 |

in Region 4 with $x_1(0)= x_2(0)=0.1$.

(b) Oscillating output waveforms corresponding to template

A = | 1.01 | 2 | -1.01 |

in Region 1 with $x_1(0)= x_2(0)=0.1$.

Observe that the CNN in Fig.18(a) is stable while the other in Fig.18(b) is unstable.

Proof of theorem 4.

Without loss of generality, let us assume a<-1 and a*>1. Suppose there is an equilibrium point such that $|x_i|\geq 1$ for all i. Assume $x_1\geq 1$, then

$$\dot{\mathbf{x}}_1 = - x_1 + 2\, y_1 + a\, y_2 = - x_1 + 2 + a\, y_2 = 0$$

Since $2-x_1 \leq 1$, we have $ay_2 = - (2-x_1) \geq -1$. If $y_2 = 1$ then $ay_2 < -1$, which leads to a contradiction. Hence, $y_2 = -1$, i.e., $x_2 \leq -1$

Similarly,

$$\dot{\mathbf{x}}_2 = - x_2 + 2\, y_2 + a^*\, y_1 + ay_3 = - x_2 - 2 + a^* + a\, y_3 = 0$$

$$- x_2 - 2 + a^* \geq 1-2+1 = 0 \Rightarrow a\, y_3 \leq 0$$

If $y_3 = -1$ then $ay_3 > 1$, which yields a contradiction. So, $y_3 = 1$ and $x_3 \geq 1$. Similarly, we find $x_4 \leq -1$, $x_5 \geq 1$, etc.

So, we have two possibilities:

$$x_{n-2} \leq -1, \qquad x_{n-1} \geq 1, \qquad x_n \leq -1$$

or

$$x_{n-2} \geq 1, \qquad x_{n-1} \leq -1, \qquad x_n \geq 1$$

In the first case

$$\dot{\mathbf{x}}_n = -x_n + 2y_n + a^* y_{n-1} = -x_n - 2 + a^* = 0$$
$$x_n = a^* - 2 > -1, \text{ which leads to a contradiction.}$$

A similar proof applies for the second case.

So, the equilibrium point for this system with $|x_i| \geq 1$ for all i does not exist. Hence, an equilibrium point for this system must satisfy $|x_i| < 1$ for some i. It can be shown that such an equilibrium point is unstable.

Sketch of proof of theorem 5.

We will only show that any binary pattern is the output of some *stable* equilibrium point. Consider a binary output $\{ b_1, b_2, ..., b_n \}$ where $b_i \in \{-1, 1\}$. We need to show that there exists an equilibrium point $(x_1, ..., x_n)$ such that $f(x_i) = b_i$. Stability follows from the fact that the Jacobian matrix at this equilibrium point is

$$\begin{bmatrix} -1 & & & \\ & \ddots & & 0 \\ & & \ddots & \\ & 0 & & \ddots \\ & & & -1 \end{bmatrix}$$

Since $b_i \in \{-1, 1\}$, this means that $|x_i| \geq 1$. In this case the state equation can be written as:

$$\dot{x}_1 = -x_1 + 2y_1 + ay_2 = -x_1 + 2b_1 + a b_2 = 0$$
$$x_1 = 2b_1 + ab_2$$

$$\dot{x}_i = -x_i + 2y_i + a^* y_{i-1} + ay_{i+1}$$
$$= -x_i + 2b_i + a^* b_{i-1} + ab_{i+1} = 0$$
$$x_i = 2b_i + a^* b_{i-1} + ab_{i+1} \quad , \quad \text{for } 2 \leq i \leq n-1.$$

$$\dot{x}_n = -x_n + 2y_n + a^* y_{n-1}$$
$$= -x_n + 2b_n + a^* b_{n-1} = 0$$
$$x_n = 2b_n + a^* b_{n-1}$$

Now we need to show that $f(x_i) = b_i$

If $b_1 = 1$ then $x_1 = 2 + ab_2$. Since $|a| < 1 \Rightarrow |ab_2| < 1$, it follows that $x_1 \geq 1$
If $b_1 = -1$ then $x_1 = -2 + ab_2 \leq -1$. Hence, $f(x_1) = b_1$.

Consider next $2 \le i \le n-1$. If $b_i = 1$ then $x_i = 2 + a^* b_{i-1} + a b_{i+1}$. Since $|a| + |a^*| \le 1$, we have $| a^* b_{i-1} + a b_{i+1} | \le |a| + |a^*| \le 1$, and hence $x_i \ge 1$.

Similarly, if $b_i = -1$ then $x_i \le -1$. Consequently $f(x_i) = b_i$. We can also show $f(x_n) = b_n$ so we have found such an equilibrium point which outputs the binary pattern b_i.

Proof of theorem 6.

We will only prove the case in region 7 where a>1. Suppose a>1 and a*>0. Since the template is sign-symmetric, we can apply the complete stability theorem 2 to show that it's stable. It remains to show that there are only 2 stable equilibrium points, whose output is either

W	W	W	W	W	W	W	W	W	W

or

B	B	B	B	B	B	B	B	B	B

We know that a stable equilibrium point must satisfy $|x_i| \ge 1$ for all i.

$$\dot{x}_1 = - x_1 + 2 y_1 + a y_2 = 0$$

Since a>1 it's easy to show that if $y_2 = 1$ then $x_1 > 1$. If $y_2 = -1$ then $x_2 < -1$, so $y_1 = y_2$.

$$\dot{x}_2 = - x_2 + 2 y_2 + a^* y_1 + a y_3$$
$$= - x_2 + (2 + a^*) y_2 + a y_3 = 0$$

Again it's easy to show that $y_2 = y_3$, so we must have $y_1 = y_2 = y_3 = y_4 = ... = y_n$. It follows that

W	W	W	W	W	W	W	W	W	W

and

B	B	B	B	B	B	B	B	B	B

are the output of the only two *stable* equilibrium points.

The proof of theorem 7 is similar to that of theorem 6.

The Venn diagram in Fig.19 illustrates the relationship between the various classes of templates we have discussed so far.

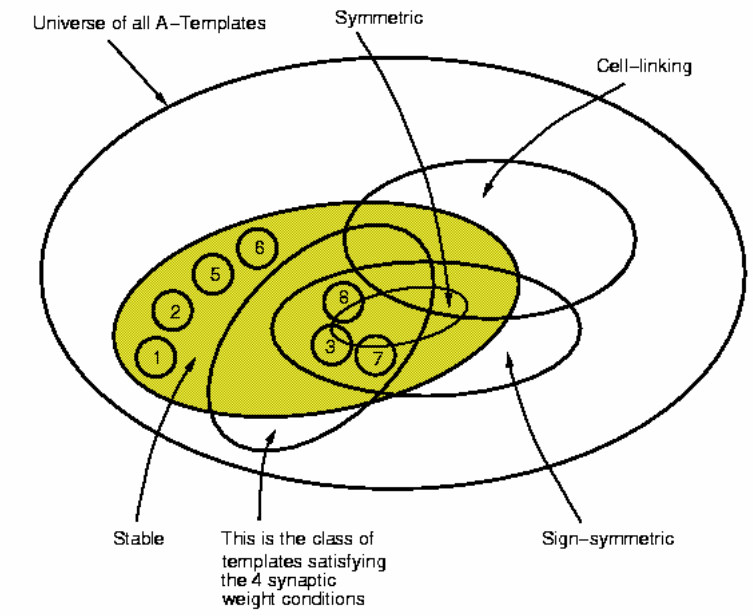

Fig.19 Venn diagram illustrating the relationship between classes of templates. The number corresponds to the regions in Figure 17.

Appendix to Chapter 8

The theorems in this section rely on the convergence results of Hirsch and the equivalent transformation results of Chua and Roska[17] and Chua and Wu[18].

Theorem A.1:[1][19]

Consider the system

$$\dot{\mathbf{x}} = \mathbf{F}(\mathbf{x})$$

Assume that for each **x** the Jacobian matrix D**F** is *irreducible*[20] and its off-diagonal elements are nonnegative. Suppose all trajectories remain bounded. Then for all initial conditions in a full measure set, the corresponding trajectories approach the set of equilibrium points.

Theorem A.2:[2][8]

Consider a CNN with time-invariant input and bias:

$$\dot{\mathbf{x}} = -\mathbf{x} + \hat{A}\, f(\mathbf{x}) + \hat{B}\, \mathbf{u} + \mathbf{z} \qquad \textbf{(A1)}$$

Let

$$A = \begin{bmatrix} a & b & c \\ d & e & f \\ g & h & i \end{bmatrix}$$

Then there exist $\hat{B}_1$, $\hat{B}_2$, $\hat{B}_3$ and $\mathbf{z}_1$, $\mathbf{z}_2$, $\mathbf{z}_3$ such that each of the following 3 systems

$$\dot{\mathbf{x}} = -\mathbf{x} + \hat{A}_1 f(\mathbf{x}) + \hat{B}_1 \mathbf{u} + \mathbf{z}_1$$
$$\dot{\mathbf{x}} = -\mathbf{x} + \hat{A}_2 f(\mathbf{x}) + \hat{B}_2 \mathbf{u} + \mathbf{z}_2$$
$$\dot{\mathbf{x}} = -\mathbf{x} + \hat{A}_3 f(\mathbf{x}) + \hat{B}_3 \mathbf{u} + \mathbf{z}_3$$

is *topological conjugate* to system (A1), where $\hat{A}_1$, $\hat{A}_2$, and $\hat{A}_3$ are given by:

---

[17] L.O. Chua and T. Roska, "Stability of a class of nonreciprocal cellular neural networks", IEEE Trans. on Circuits and Systems, vol. 37, pp.1520-1527.

[18] L.O. Chua and C.W. Wu, "On the universe of stable cellular neural networks," Int. J. Circuit Theory and Application, vol.20, 497-512, 1992

[19] M.W. Hirsch, "System of differential equations that are competitive or cooperative II: Convergence almost everywhere," SIAM Math. Anal., vol.16, no.3, May 1985, pp.423-439.

[20] A *permutation* matrix P is a matrix whose entries consists of 0 or 1 such that each row or column contains only one "1". A matrix D is *irreducible* if there exists a *permutation* matrix P such that PDP^T is of the form

5	μ
⊗	5

where "μ" denotes a matrix with all zero entries, "5" denotes a nonzero matrix, and "⊗" denotes any matrix.

$$A1 = \begin{bmatrix} -a & b & -c \\ -d & e & -f \\ -g & h & -i \end{bmatrix}$$

$$A2 = \begin{bmatrix} -a & -b & -c \\ d & e & f \\ -g & -h & -i \end{bmatrix}$$

$$A3 = \begin{bmatrix} a & -b & c \\ -d & e & -f \\ g & -h & i \end{bmatrix}$$

Roughly speaking, topological conjugacy means that the dynamics are qualitatively the same. In particular, stability properties are preserved under topological conjugacy.

LaSalle's invariance principle

Consider the autonomous system

$$\dot{\mathbf{x}} = \mathbf{f}(\mathbf{x}), \qquad \mathbf{x} \in R^n$$

Let $V(\mathbf{x})$ be a continuously differentiable function from R^n into R. Let S be an arbitrary set in R^n. Suppose $\dot{V} = \nabla V \bullet \mathbf{f}(\mathbf{x})$ does not change sign in S. Define

$$E = \{\mathbf{x}: \dot{V}(\mathbf{x}) = 0, \mathbf{x} \in \overline{S}\}$$

where $\overline{S}$ denotes the closure of S. Let M be the largest invariant set in E. Then M is a *closed* set and for all solutions remaining in S for all $t \geq 0$, x(t) approaches the closed invariant set M, or "∞", i.e., $M \cup \{\infty\}$, where "$\cup$" denotes "set union" and $\{\infty\}$ denotes the point at ∞.